Appl Phys B (2010) 99: 135–140
DOI 10.1007/s00340-009-3790-7

Applied Physics B
Lasers and Optics

Multi-wavelength diode-pumped Nd:LGGG picosecond laser

A. Agnesi · F. Pirzio · G. Reali · A. Arcangeli · M. Tonelli · Z. Jia · X. Tao

Received: 22 July 2009 / Revised version: 30 September 2009 / Published online: 1 November 2009

Abstract Laser operation near 1.06 μm by a diode-pumped Nd:$(Lu_xGd_{1-x})_3Ga_5O_{12}$ (Nd:LGGG) disordered crystal has been investigated. Cw oscillation, with a slope efficiency as high as 61% and 230 mW output power, was achieved with 400 mW absorbed power from a 1-W laser diode. Stable passive mode locking with single- or multi-banded spectrum was obtained with a semiconductor saturable absorber mirror (SAM) and a single-prism, dispersion-compensated cavity. Fourier limited pulses with duration ≈3–9 ps and output power ≈40 mW were generated at three well-defined laser transitions in the range 1062–1067 nm.

PACS 42.70.Hj · 42.55.Xi · 42.65.Re

1 Introduction

Diode-pumped Nd-doped lasers based on disordered crystalline hosts, such as Nd:CNGG [1–3], Nd:CNLGG [4], and Nd:CTGG [5], have attracted significant attention lately because of their simultaneous multi-wavelength emission in Q-switching and mode-locking regimes, within a spectral range of few nanometers. Such laser pulses at different wavelengths can be properly synchronized, allowing for potential THz generation by difference frequency mixing in suitable nonlinear optical media [6, 7]. Optical generation of THz beams is an extremely active research field [8], with many important applications, such as bio-diagnostics and security.

Compared with optical parametric oscillators, that become increasingly unstable as nearly-degenerate signal and idler frequencies are approached, disordered laser crystals present closely spaced, yet well defined, emission wavelengths arising from laser transitions of Nd^{3+} ions in specific sites. It is worth noticing that such a relatively sparse distribution of transition frequencies seems to prevent successful mode locking over bandwidths of several nanometers, contrary to what fluorescence spectra would suggest at first sight. Indeed, the shortest pulse generated by passive mode locking was reported for Nd:CNLGG to be 900-fs long [2], corresponding to a spectral band of 1.8 nm, against a reported ≈15-nm emission band of the laser material [9]. This contrasts solid-state laser materials with significant inhomogeneous broadening and a more continuous distribution of laser transition frequencies, such as Nd:glass, that allow instead for almost complete locking of resonant longitudinal modes within the gain bandwidth, producing femtosecond pulses with spectral width comparable with the whole fluorescence emission range [10].

However, multi-wavelength pulse operation of few picosecond duration is very attractive for THz generation owing to a more favorable damage threshold of nonlinear crystals used for this peculiar difference mixing application with respect to nanosecond Q-switched lasers.

We report on a diode-pumped mode-locked Nd:LGGG laser oscillator that generates either a single 9-ps pulse at 1062.2 nm, or synchronized pulses at 1062.2, 1066.6, and 1067.1 nm, with the shortest pulse width being estimated

A. Agnesi (✉) · F. Pirzio · G. Reali
INFN Sez. di Pavia and Dipartimento di Elettronica, dell'Università di Pavia, Via Ferrata 1, 27100 Pavia, Italy
e-mail: antonio.agnesi@unipv.it

A. Arcangeli · M. Tonelli
CNR NEST and Dipartimento di Fisica, dell'Università di Pisa, Largo B. Pontecorvo, 3, 56127 Pisa, Italy

Z. Jia · X. Tao
State Key Laboratory of Crystal Materials, Shandong University, Ji'nan 250100, PR China

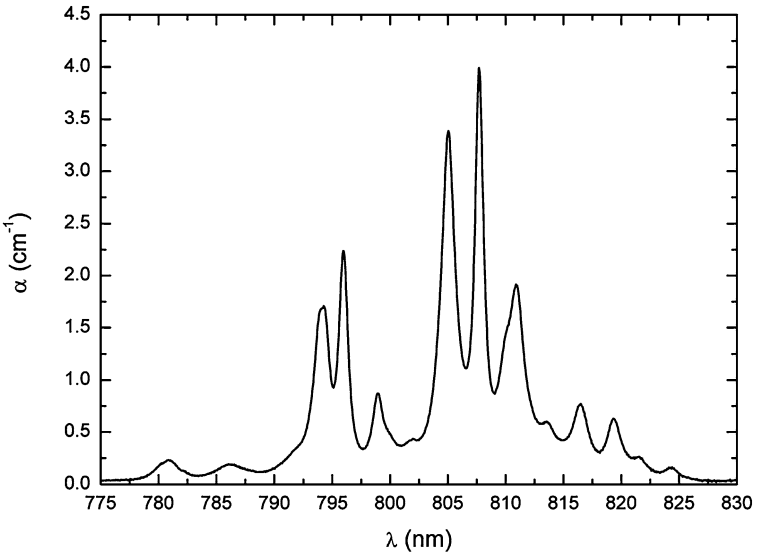

Fig. 1 Absorption spectrum of Nd:LGGG at room temperature

≈3.0–4.3 ps. Difference frequencies at 0.13, 1.2, 1.3 THz could be generated in this case with a suitable nonlinear crystal.

2 Crystal growth and spectroscopic analysis

A Nd:LGGG crystal with the dimensions of $\Phi 21 \times 30$ mm^2 was grown along the ⟨111⟩ orientation by the Cz method at the Institute of Crystal Materials, Shandong University, China, and detailed information can be found in Ref. [11]. Here the key information about the crystal growth and structural characterization is summarized for the convenience of reading the following.

During the process of crystal growth special attention has been given to the growing atmosphere ($N_2 + 20$ vol% CO_2) to reduce the decomposition of Ga_2O_3. In addition, the rate of rotation was also one of the key parameters to obtain a flat interface shape, and it ranged from 15 to 20 rpm depending on the crystal growing parts, such as neck, shoulder, column, and tail. We have performed the X-ray diffraction measurement and found that the as-obtained Nd:LGGG crystal was cubic with a unit cell axis length of $a = 1.2361$ nm, which was smaller than that of Nd:GGG crystal (1.2376 nm, JCPDS diffraction file of GGG: No. 13-0493). The Nd^{3+} concentration was determined by X-ray fluorescence to be about 0.53 at.% in this crystal.

The measurements of absorption spectra at room temperature were made by a Varian Cary 500 spectrophotometer with the resolution of 0.15 nm (Fig. 1) and showed a broad absorption region with several peaks between 790 nm and 820 nm, the most important region for laser diode pumping (the transitions are $^4I_{9/2} \rightarrow {}^2H_{9/2} + {}^4F_{5/2}$. The most relevant peak values are those of 4 cm^{-1} at 807.7 nm (fwhm = 1.0 nm), 3.4 cm^{-1} at 805.0 nm (fwhm = 1.5 nm) and 2.2 cm^{-1} at 796.0 nm (fwhm = 1.2 nm). The absorption properties have been also investigated at 10 K with a resolution of 0.06 nm, where we found that the spectrum shows eight nearly isolated absorption peaks between 780 nm and 810 nm, due to the depopulation of the upper Stark sublevels of the ground state: the main absorption peaks are centered at 807.26 nm, 804.64 nm and 795.60 nm.

Since our crystal is isomorphous to GGG (Gadolinium Gallium Garnet) by substituting a fraction of Gd atoms with Lu atoms, we expect to observe a multi-site structure, as happens for GGG [12]. To focus on this, we investigated the fluorescence of the $^4F_{3/2} \rightarrow {}^4I_{11/2}$ transition at low temperature (10 K). The maximum resolution in our experimental apparatus was 0.2 nm in order to obtain a good signal to noise ratio. In Fig. 2(a) we show the luminescence at 10 K operating temperature exciting the sample at 807.2 nm with a tunable cw Ti–Sa laser: this wavelength is inside the bandwidth of the pumping diode laser used for excitation of the Nd:LGGG laser discussed in Sect. 3. The asymmetric broadening of the emission around 1065 nm suggests the presence of two nonresolved lines, as shown in Fig. 2(b) by the fitting with two Gaussian curves, peaked at 1065.5 nm and 1066.1 nm: this aspect will be emphasized in Sect. 3 of this paper, when laser action is discussed. With these two lines, the transitions in this band reach the number of 7, one more than expected theoretically: this is evidence of the multi-site characteristic of the host.

We detected the emission at room temperature for the relevant laser transitions around 1060 nm, in order to calculate the stimulated emission cross section by the so-called integral β–τ method [13] and we also measured the lifetime of the $^4F_{3/2}$ multiplet (≈250 μs from 10 K to room temperature). We obtained the peak values of 1.1×10^{-19} cm^2 at 1062.3 nm, and 5.8×10^{-20} cm^2 at 1066.8 nm, about five

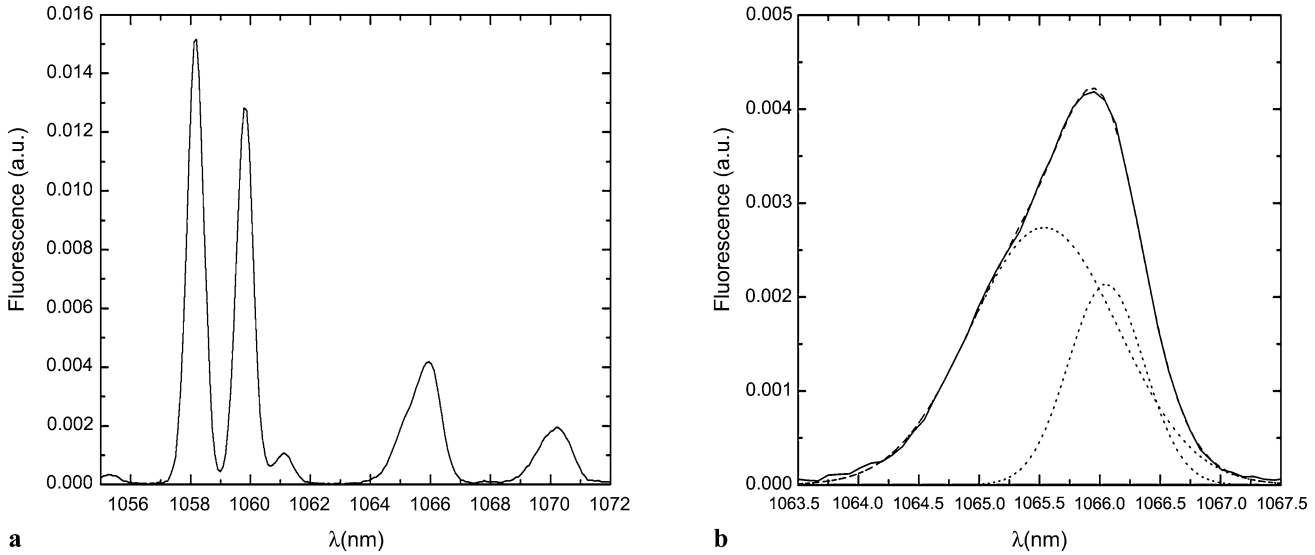

Fig. 2 Multi-site structure of Nd: LGGG shown by the luminescence at 10 K after pumping at 807.2 nm. (**a**) Whole $^4F_{3/2} \rightarrow {}^4I_{11/2}$ band. (**b**) Particulars of the emission around 1066 nm (*solid line*), fitted by two Gaussian curves centered at 1065.5 nm and 1066.1 nm (*dotted line*). *The dashed line* is the sum of the two Gaussian curves and is almost superposed to *the solid line* indicating the experimental result

times lower than the cross section in Nd:YAG in the same wavelength region [13].

3 Experiments

The Nd:LGGG crystal was tested in order to assess its laser characteristics. The laser cavity for cw operation was the X-folded resonator shown in Fig. 3. The pump diode was a $50 \times 1\ \mu m^2$ high-brightness commercial emitter, with maximum output power 1 W at 808 nm. It was collimated by an 8-mm focal aspheric lens L1, expanded by a factor 15 in the slow-axis direction with a cylindrical lens telescope (C1, C2), and eventually focused in the Nd:LGGG sample by a 80-mm focal achromat L2. The pump spot size in air, measured with a CCD camera, was $W_x \times W_y \approx 21 \times 11\ \mu m^2$, along the (horizontal) slow and fast axis, respectively.

The 4.5-mm long Nd:LGGG crystal was placed inside the resonator oriented at Brewster angle to minimize the losses. Owing to the relatively small absorption coefficient at 808 nm and its narrow peak, comparable to the laser diode spectral width (≈1 nm), the pump power absorbed by the laser crystal was limited to 400 mW.

In this experimental run, the crystal was not actively cooled; however, we did not observe any thermal problem at such low pump levels.

The waist radius of the cw X-shaped cavity within the Brewster-oriented crystal was $70 \times 37\ \mu m^2$. The distances between the cavity mirrors were M1 − M2 = 107 mm, M2 − M3 = 350 mm, M1 − OC = 340 mm. We achieved a very efficient cw operation, with a slope efficiency as high

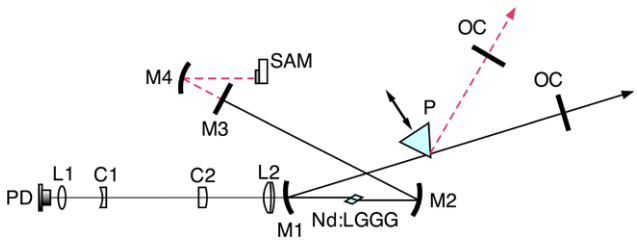

Fig. 3 Resonator layout. *PD*: pump laser diode; *L1*: aspheric lens; *L2*: achromatic lens; *C1, C2*: cylindrical lenses (15× telescope); *M1, M2*: concave mirrors, 100-mm curvature, HR at 1064 nm, high transmissivity at 800–810 nm; *M3*: flat mirror, HR; *M4*: concave mirror, HR with 75-mm radius of curvature; *P*: SF10 Brewster-cut prism; *OC*: output coupler mirror, 30′ wedge

as 61% using an output coupler transmittivity $T_{oc} = 10\%$. Almost the same slope efficiency but a maximum output power of 230 mW was obtained with the optimum $T_{oc} = 5\%$ (Fig. 4).

For the mode-locking operation, the flat high-reflectivity (HR) mirror M3 was replaced by an additional focusing mirror M4 (75-mm radius of curvature), and a semiconductor saturable absorber mirror (SAM) with either 1% or 2% nominal absorption (BATOP GmbH) was used as the cavity end mirror. Mirror separations of this modified laser setup were M1 − M2 = 107 mm, M2 − M4 = 350 mm, M1 − OC = 340 mm, M4 − SAM ≈ 36 mm.

A single SF10 Brewster prism P was used for dispersion compensation, as in Ref. [14]. At 240 mm from the mirror M1, its effect on the cavity dispersion was equivalent to that of a pair of SF10 prisms separated by ≈60 cm. This choice definitely reduces the complexity of the resonator, making

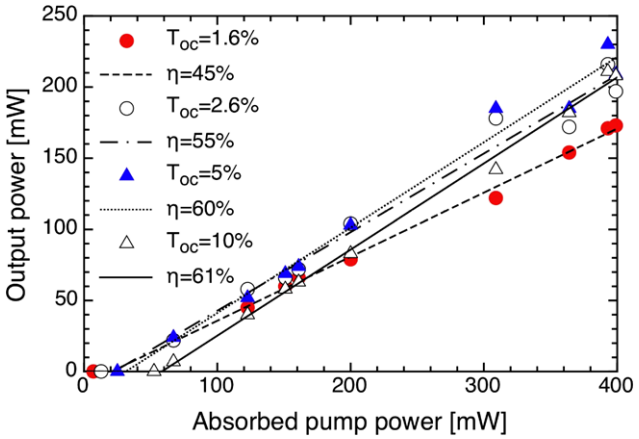

Fig. 4 Performance of Nd:LGGG in cw operation, with several output couplers

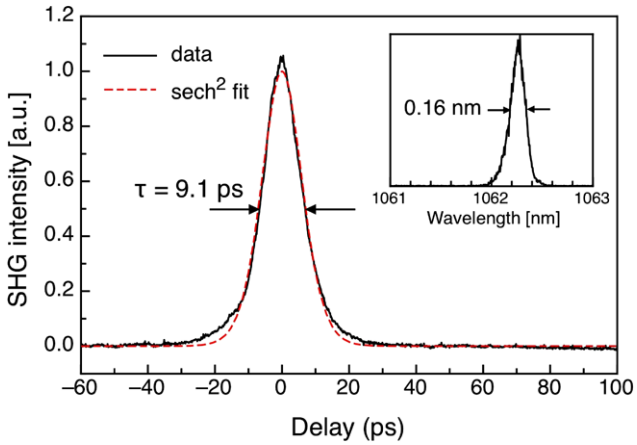

Fig. 5 Noncollinear second-harmonic autocorrelation and spectra (*inset*) of mode-locking pulses at a single wavelength (1062.2 nm). Also shown is the autocorrelation best-fit curve corresponding to a sech^2 pulse shape

it more compact and simpler to operate than in previously reported two-prisms compensation arrangements of mode-locked disordered laser crystals [2, 4, 5]. The purpose of the intra-cavity prisms in these lasers is twofold:

(i) (standard) stabilization of soliton-like pulses with net negative dispersion, although rarely in femtosecond domain, and
(ii) synchronization of multi-wavelength picosecond pulses.

Output couplers with small transmittivity ($T_{oc} = 0.8\%$ and 1.6%) were used in this case, to reduce the critical pulse energy required to stabilize cw mode locking [15].

A commercial autocorrelator (Femtochrome FR-103XL) and an optical spectrum analyzer (ANDO AQ6317B) were used to characterize the pulse width and the optical spectrum.

The shortest mode-locking pulses were observed with the 2% SAM (1.2% saturable loss) and 0.8% OC. By tilting the OC horizontally, we could control the wavelength emission in mode-locking regime, with an approximately constant output power ≈40 mW.

A first operation with single $\tau = 9.1$ ps pulse (intensity fwhm) and $\Delta\lambda = 0.16$ nm spectrum (Fig. 5) was observed at the main transition line of 1062.2 nm (nearly Fourier limited, $\tau \times \Delta\nu = 0.39$).

In a second operating regime, the spectral shape hinted at the existence of two synchronized pulses at 1066.6 and 1067.1 nm, yielding the minimum pulse duration, which we evaluated in the following way. Figure 6 shows the 6.3-ps wide autocorrelation and the spectrum, which suggests two slightly separated pulse frequencies simultaneously oscillating. Indeed, these two wavelengths, corresponding to much longer picosecond pulses, were clearly separated and overlapped gradually only when optimizing the prism insertion and the cavity alignment. The usual sech^2 fit of the autocorrelation would yield 4.3 ps fwhm. However, given the

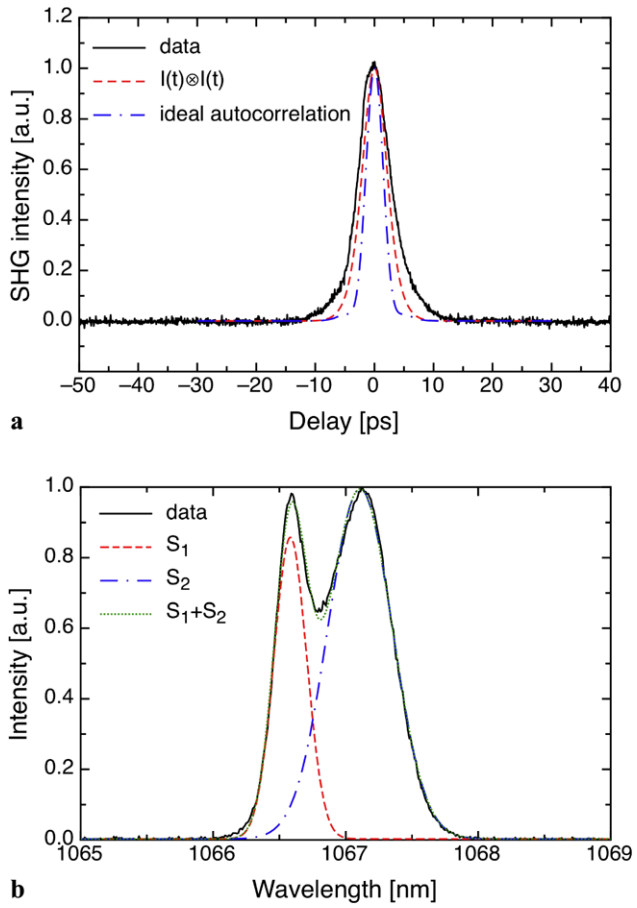

Fig. 6 (**a**) Noncollinear second-harmonic autocorrelation in dual-wavelength regime. Also shown are the autocorrelation curve corresponding to the total intensity $I(t) = I_1(t) + I_2(t)$ of Fourier limited pulses with spectral density $S_1(\lambda)$ and $S_2(\lambda)$, with $\tau = 5.7$ ps and 3.0 ps (intensity fwhm), and the ideal autocorrelation trace corresponding to the whole spectrum supposed to be perfectly phase-locked (i.e. Fourier limited). (**b**) Spectrum decomposition of mode-locking pulses at two wavelengths (1066.6 and 1067.1 nm)

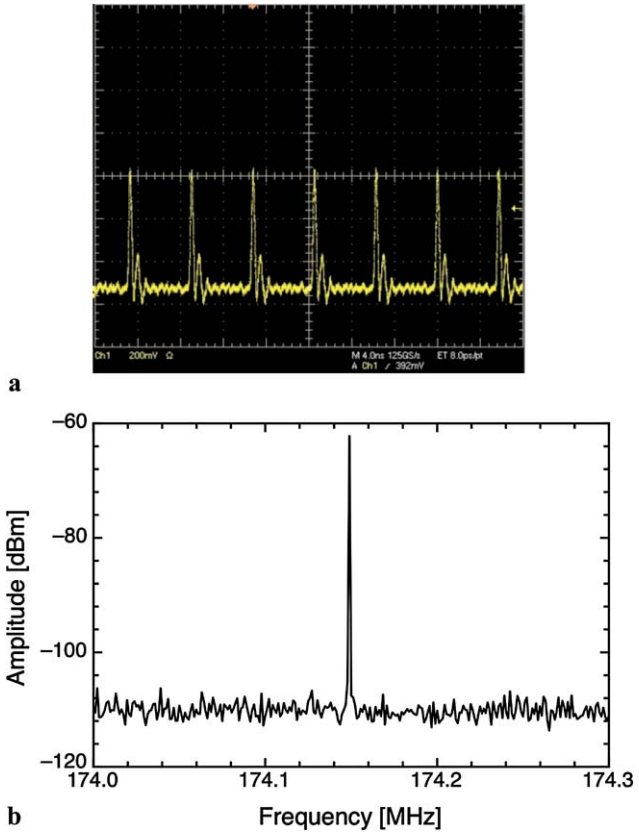

Fig. 7 Oscilloscope trace (measured by a 1-GHz oscilloscope Tektronix TDS5104B) and RF spectrum (measured by a 3-GHz analyzer Agilent N9320B) of the two-wavelength mode-locking regime

peculiar spectral shape one might rather compare the intensity autocorrelation of the inverse Fourier transform of the spectrum, which turns out to be ≈3.4 ps (envelope of pulse intensity ≈2.5 ps fwhm), with the measured autocorrelation fwhm ≈6.3 ps fwhm. This would suggest a product $\tau \times \Delta\nu$ about 1.9 times the Fourier limit. Alternatively, one might consider the observed spectrum as the sum of contributions from two distinct spectral features, which we chose to model as Gaussian profiles $S_1(\lambda)$ and $S_2(\lambda)$ in Fig. 6(b).

It is worth noticing that the laser transitions at room temperature are red-shifted, as happens for extensively characterized materials such as Nd:YAG, whose emission peak shifts by 4 pm/°C [16].

The inverse Fourier transforms of $S_1^{1/2}(\nu)$ and $S_2^{1/2}(\nu)$ correspond to Fourier limited pulses $I_1(t)$, $I_2(t)$ of 5.6-ps and 3.0-ps duration fwhm, respectively (the shorter pulse containing 70% of the total energy). The calculated autocorrelation $I(t) \otimes I(t)$ of the total intensity $I(t) = I_1(t) + I_2(t)$ yields a result in fair agreement with the measured autocorrelation (Fig. 6(a)), corroborating our guess. The slight discrepancy may be due to slightly non-Fourier limited pulses (by a factor ≈1.2) from S_1 and S_2, which is significantly smaller than the factor of 1.9 initially inferred when considering complete phase locking of the spectrum.

In principle one should autocorrelate the total intensity corresponding to the sum of the pulse amplitudes: in addition to the pure intensity autocorrelation this gives frequency-beating cross-correlation terms as well as high-frequency terms, which we did not detect. A possible explanation is that phase noise and timing jitter ≈1 ps typical of passively mode-locked solid-state lasers [17] average to zero such correlation contributions, leaving only the intensity term.

The oscilloscope trace and the RF spectrum of this synchronous two-wavelength regime are displayed in Fig. 7, marking the stability of the mode locking.

A third mode-locking operating regime corresponded to all three pulse wavelengths running synchronously, with a three-pulse autocorrelation width still mostly shaped by the shorter, ≈3-ps pulse at 1067.1 nm: the energy is distributed among the pulses at 1062.2, 1066.6, 1067.1 nm in the ratios 17%, 25%, 58% according to the individual spectral areas.

We notice that the transverse beam displacement at the SAM was ≈2% of the mode radius for each nm of wavelength separation, therefore not significant in this case to compromise pulse synchronization. Also, the spatial dispersion at the output coupler was comparably small, definitely not affecting potential extra-cavity frequency mixing setups.

4 Conclusions

Highly efficient cw operation of the disordered Nd:LGGG crystal has been reported. Furthermore, passive mode locking with a commercial SAM device has been investigated. Single- and multi-wavelength oscillation with picosecond pulses has been achieved with a single-prism, dispersion-compensated resonator. Our results confirm the difficulty of disordered Nd-doped crystals to yield femtosecond pulse mode locking, despite the relatively broad fluorescence spectra extending over several nanometers. Instead, pulses at several distinct wavelengths are allowed to oscillate simultaneously, owing to the dispersion-compensated resonator design and to the saturable absorber that favors pulse synchronism in order to minimize losses.

A particular pair pulse oscillation, with a small central wavelength separation of 0.53 nm, is proposed to be understood as two intensity-correlated and Fourier limited pulses, with durations of 3.0 ps and 5.7 ps. Considering the wavelength separations in multi-color oscillation regimes, this laser might be employed (also taking advantage of powerful, readily available broad-band fiber amplifiers) to generate THz beams through difference frequency nonlinear interactions at 1.2 and 1.3 THz, as well as millimetric waves at 0.13 THz.

References

1. A. Agnesi, S. Dell'Acqua, A. Guandalini, G. Reali, F. Cornacchia, A. Toncelli, M. Tonelli, K. Shimamura, T. Fukuda, IEEE J. Quantum Electron. **37**, 304 (2001)
2. G.Q. Xie, D.Y. Tang, H. Luo, H.J. Zhang, H.H. Yu, J.Y. Wang, X.T. Tao, M.H. Jiang, L.J. Qian, Opt. Lett. **33**, 1872 (2008)
3. H. Yu, H. Zhang, Z. Wang, J. Wang, Y. Tu, Z. Shi, X. Zhang, M. Jiang, Opt. Lett. **34**, 151 (2009)
4. G.Q. Xie, D.Y. Tang, W.D. Tan, H. Luo, H.J. Zhang, H.H. Yu, J.Y. Wang, Opt. Lett. **34**, 103 (2009)
5. G.Q. Xie, D.Y. Tang, W.D. Tan, H. Luo, S.Y. Guo, H.H. Yu, H.J. Zhang, Appl. Phys. B **95**, 691 (2009)
6. D. Creeden, J.C. McCarthy, P.A. Ketteridge, P.G. Schunemann, T. Southward, J.J. Komiak, E.P. Chiklis, Opt. Express **15**, 6478 (2007)
7. K.L. Vodopyanov, J.E. Schaaar, P.S. Kuo, M.M. Fejer, A. Lin, J.S. Harris, W.C. Hurlbut, V.G. Kozlov, D. Bliss, C. Lynch, in *Advanced Solid-State Photonics, OSA Technical Digest Series (CD)* (Optical Society of America, 2008), paper WD2
8. G.Kh. Kitaeva, Laser Phys. Lett. **5**, 559 (2008)
9. Yu.K. Voronko, A.A. Sobol, A.Ya. Karasik, N.A. Eskov, P.A. Rabochkina, S.N. Ushakov, Opt. Mater. **20**, 197 (2002)
10. J. Aus der Au, D. Kopf, F. Morier-Genoud, M. Moser, U. Keller, Opt. Lett. **22**, 307 (1997)
11. Z. Jia, X. Tao, H. Yu, C. Dong, J. Zhang, H. Zhang, Z. Wang, M. Jiang, Opt. Mater. **31**, 346 (2008)
12. I. Vergara, A. Monteil, G. Boulon, C. Madei, Mater. Chem. Phys. **26**, 181 (1990)
13. B.F. Aull, H.P. Jenssen, IEEE J. Quantum Electron. **18**, 925 (1982)
14. D. Kopf, G.J. Spühler, K.J. Weingarten, U. Keller, Appl. Opt. **35**, 912 (1996)
15. C. Hönninger, R. Paschotta, F. Morier-Genoud, M. Moser, U. Keller, J. Opt. Soc. Am. B **16**, 46 (1999)
16. O. Kimmelma, I. Tittonen, S.C. Buchter, Appl. Opt. **47**, 4262 (2008)
17. H. Tsuchida, Opt. Lett. **24**, 641 (1999)